Global Minimizers of The Active Contour/Snake Model

X. Bresson*, S. Esedoḡlu†, P. Vandergheynst*, J.P. Thiran* and S. Osher†

* Signal Processing Institute,
Swiss Federal Institute of Technology (EPFL)
1015 Lausanne, Switzerland
{xavier.bresson,pierre.vandergheynst,jp.thiran}@epfl.ch

† Department of Mathematics,
University of California,
90095-1555 Los Angeles, CA, United States
{esedoglu,sjo}@math.ucla.edu

January 18, 2005

Abstract

The active contour/snake model [9, 2, 10] is one of the most well-known segmentation variational models in image processing. However this model suffers from the existence of local minima which makes the initial guess critical for getting satisfactory results. In this paper, we propose to solve this problem by finding global minimizers of the active contour model following the original work of Chan, Esedoḡlu and Nikolova [4]. Our approach uses the weighted total variation norm to link the standard active contour segmentation model with the denoising model of Rudin-Osher-Fatemi [15] and the Chan-Vese active contour segmentation models [5, 18] based on the Mumford-Shah functional [12].

1 Introduction

The segmentation problem is fundamental in the computer vision and image processing fields since it is a core component towards e.g. automated

vision systems and medical applications. Its aim is to find a partition of an image into a finite number of semantically important regions. Various variational and partial differential equations (PDEs) methods have been proposed to extract objects of interest in images such as the well-known active contour/snake model defined by Kass *et al.* in [9]. This method has been widely used in different image processing applications such as in medical imaging to extract anatomical structures [11, 20, 8].

Following this first model of active contours, Caselles *et al.* in [2] and Kichenassamy *et al.* in [10] have proposed the following minimization problem invariant w.r.t. the curve parametrization:

$$\min_C E_{gac}(C) = \oint_0^{L(C)} g \; ds, \tag{1}$$

where ds is the Euclidean element of length, $L(C)$ is the length of the curve C and g is an edge detecting function that vanishes at object boundaries such as:

$$g = \frac{1}{1 + \beta |\nabla f_\sigma|^2}, \tag{2}$$

where f is the original image, f_σ is a smoothed version of the original image and β is an arbitrary positive constant.

The calculus of variations provides the Euler-Lagrange equation of the functional E_{gac} and the gradient descent method gives the flow that minimizes E_{gac} (see [2]):

$$\partial_t C = (\kappa g - \langle \nabla g, \mathcal{N} \rangle) \mathcal{N}, \tag{3}$$

where κ is the curvature and $\mathcal{N}$ the normal to the curve. Osher and Sethian have introduced in [14] the implicit and intrinsic level set representation of contours to efficiently solve the contour propogation problem and to deal with topological changes. Equation (3) can be written in the level set form:

$$\partial_t \phi = \left(\kappa g + \langle \nabla g, \frac{\nabla \phi}{|\nabla \phi|} \rangle \right) |\nabla \phi|, \tag{4}$$

where ϕ is the level set function embedding the active contour C.

The main drawback of this variational segmentation model, as many other variational models in image processing, is the existence of local minima

in the energy E_{gac}. Local minima are undesirable in optimization problems since they provide unsatisfactory results. For example, the initial active contour (embedded in a level set function) on Figure 1(a) can not fully segment both objects, Figure 1(b), because it gets stuck in a local minimum.

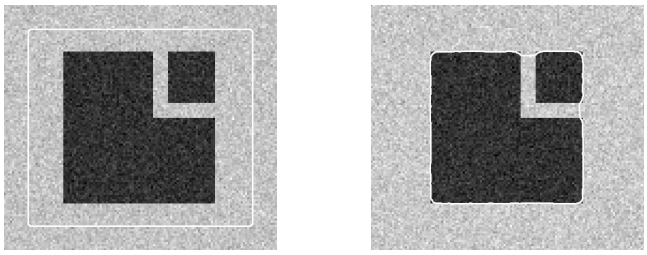

(a) Initial Active Contour.

(b) Final Active Contour.

Figure 1: Standard active contour fails to segment both objects.

The approach defined by Chan, Esedoḡlu and Nikolova in [4] proposes a solution to overcome this limitation. In their paper, image segmentation and image denoising are closely related. Image denoising aims at removing noise in images while keeping main features such as edges and textures. Two important variational models of image denoising are the Rudin-Osher-Fatemi (ROF) model [15] and the Mumford-Shah model [12] (even if the Mumford-Shah model is primarily a segmentation model). In [19, 13], Vese and Osher have shown that the level set method links the ROF and the Mumford-Shah models.

The authors in [4] proposed a method to find global minimizers of two well-known denoising and segmentation models. The first model is a binary image denoising model which removes the geometric noise in a given shape. And the second example is the powerful model of *active contours without edges* of Chan and Vese [5].

In this paper, we propose three algorithms based on the work of Chan, Esedoḡlu and Nikolova [4] to find global minimizers of the standard active contour/snake model. Our first approach is based on the ROF model where the total variation (TV) norm of the unknown function is replaced by the weighted TV-norm and the L^2-norm for the fidelity term is changed into the

L^1-norm [6]. We will show that the global minimizers of this new energy are the global minimizers of the active contour model subject to an intensity homogeneity constraint. Then, we will reconcile the standard active contours and the Chan-Vese active contours defined from the Mumford-Shah functional in a global minimization framework.

2 Global Minimization of the Active Contour Model based on the ROF Model

The Rudin-Osher-Fatemi model defined in [15] is one of the most famous and powerful variational and PDE based image denoising models. This denoising technique removes the noise while preserving the edges in images. The minimization problem of the convex ROF energy is as follows:

$$\min_u E_{ROF}(u,\lambda) = \int_\Omega |\nabla u| + \lambda \int_\Omega (u-f)^2\, dx, \tag{5}$$

where $\Omega \subset \mathbf{R}^N$ is an open set, f is a given (possibly noisy) image and λ is an arbitrary positive parameter related to the scale of observation of the solution.

Based on the works [3, 4], we propose to minimize the following convex energy defined for any given observed image $f \in L^1(\Omega)$ and any positive parameter λ:

$$E_1(u,\lambda) = \int_\Omega g|\nabla u| + \lambda \int_\Omega |u-f| dx. \tag{6}$$

The difference between the energy (6) and the ROF model (5) is the introduction of the *weighted TV-norm* of u with the weight g and the L^1*-norm* as a fidelity measure. The L^1-norm, replacing the L^2-norm square of the original ROF model, has a big impact in the minimization process since it will allow us to find global minimizers of the snake model.

In [3], Chan and Esedoḡlu have studied the differences between the standard ROF model and the ROF model that uses the L^1-norm as a fidelity measure. They have shown that L^1-norm better preserves the contrast than L^2-norm and the order in which the features disappear is completely determined in terms of the geometry (such as area and length) of the features and not in terms of the contrast. Figure 2 presents the difference between

the ROF model with L^1-norm as a fidelity measure and our model, defined by energy E_1, that uses the weighted TV-norm. The parameter λ for both models is the largest value such that the four small circles in the original image (Figure 2(a)) are removed. The difference between both models is clear, the result generated by the weighted TV-norm and the L^1 fidelity term better preserves the geometry of the original features such as the corners and the largest circle.

The weighted total variation norm of the function u with the weight function g is defined as the following way:

Definition 1: Let $\Omega \subset \mathbf{R}^N$ be an open set and $u \in L^1(\Omega)$ and let g be a positive valued continuous and bounded function in Ω. Define the weighted total variation norm of u with the weight function g by

$$TV_g(u) = \int_\Omega g|\nabla u| := \sup_{\phi \in \Phi_g} \left\{ \int_\Omega u(x) \mathrm{div}\phi(x)\ dx \right\}, \tag{7}$$

where

$$\Phi_g := \{\phi \in C^1(\Omega, \mathbf{R}) \mid |\phi(x)| \leq g, \text{ for all } x \in \Omega\}. \tag{8}$$

The coarea formula for the TV_g-norm reads as follows (Strang [17]):

$$\begin{aligned} \int_\Omega g|\nabla u| &= \int_{-\infty}^{\infty} \left(\int_{\gamma_\mu} g ds \right)\ d\mu, & (9) \\ &= \int_{-\infty}^{\infty} \mathrm{Per}_g(E_\mu := \{x : u(x) > \mu\})\ d\mu, & (10) \end{aligned}$$

where γ_μ is the boundary of the set E_μ on which $u(x) > \mu$. Hence, the term $\mathrm{Per}_g(E_\mu) = \int_{\gamma_\mu} g ds$ is the perimeter of the set E_μ weighted by the function g.

The relation between the minimization of energy (6) and the active contour/ snake model [2, 10] is as follows: If $\mathbf{1}_{\Omega_C}$ is the characteristic function of a set Ω_C whose boundary is denoted C, then

$$\begin{aligned} E_1(u = \mathbf{1}_{\Omega_C}, \lambda) &= \int_\Omega g|\nabla \mathbf{1}_{\Omega_C}| + \lambda \int_\Omega |\mathbf{1}_{\Omega_C} - f| dx, & (11) \\ &= \int_C g ds + \lambda \int_\Omega |\mathbf{1}_{\Omega_C} - f| dx. & (12) \end{aligned}$$

Hence, minimizing the energy (12) is equivalent to

$$\textit{minimize} \quad \int_C g ds = E_{gac}(C) \quad \text{(the active contour energy (1))} \ ,$$

while

$$\begin{array}{c} \text{approximating } f \text{ (in the } L^1 \text{ sense) by} \\ \text{a binary function of a set/region } \Omega_C. \end{array}$$

We now state the Theorem 1:

Theorem 1: *Suppose that $g(x) \in [0,1]$ and $f(x)$ is the characteristic function of a bounded domain in $\Omega_f \subset \Omega$, if $u_\lambda(x)$ is any minimizer of $E_1(.,\lambda)$, then for almost every $\mu \in [0,1]$ we have that the characteristic function*

$$\mathbf{1}_{\Omega_C(\mu)=\{x:u_\lambda(x)>\mu\}} \ (x), \tag{13}$$

where C is the boundary of the set Ω_C, is a global minimizer of $E_1(.,\lambda)$.

Proof. The proof of Theorem 1 is based on [16, 17, 3, 4] substituting the TV-norm by the weighted TV-norm. It basically consists of expressing the energy (6) in terms of the level sets of u and f:

$$\begin{aligned} E_1(u,\lambda) = \int_0^1 & \mathrm{Per}_g(\{x : u(x) > \mu\}) + \\ & \lambda \left| \{x : u(x) > \mu\} \triangle \{x : f(x) > \mu\} \right| \ d\mu, \end{aligned}$$

then minimizing energy (6) pointwise in μ by solving a geometry problem.

Following Theorem 1, we look for *any* minimizer of the energy E_1. Since the energy functional E_1 is convex, it does not possess local minima that are not global minima. Therefore the gradient descent method is guaranteed to find a global minimizer of the segmentation model. The minimization flow of the functional E_1 is:

$$\begin{aligned} u_t &= \mathrm{div}\left(g\frac{\nabla u}{|\nabla u|}\right) + \lambda\frac{u-f}{|u-f|}, & (14) \\ &= g \ \mathrm{div}\left(\frac{\nabla u}{|\nabla u|}\right) + \langle \nabla g, \frac{\nabla u}{|\nabla u|}\rangle + \lambda\frac{u-f}{|u-f|}, & (15) \end{aligned}$$

where the first term of the right-hand side is the curvature of the level sets of u multiplies by the weight function g, the second term is a shock term which enhances the edges and the third term of the right-hand side is a data fidelity term w.r.t. the observed image f.

Then, we discretize the evolution equation (15) according to the numerical scheme:

$$\begin{aligned}
\frac{u^{n+1}-u^n}{\delta t} = \quad & g(\sqrt{(D_x^0 f_\sigma)^2 + (D_y^0 f_\sigma)^2}) \cdot \\
& \left\{ D_x^- \left(\frac{D_x^+ u^n}{\sqrt{(D_x^+ u^n)^2 + (D_y^+ u^n)^2 + \varepsilon_1}} \right) \right. \\
& \left. + D_y^- \left(\frac{D_y^+ u^n}{\sqrt{(D_x^+ u^n)^2 + (D_y^+ u^n)^2 + \varepsilon_1}} \right) \right\} \\
+ \quad & \max(D_x^0 g, 0) \frac{D_x^- u^n}{\sqrt{(D_x^0 u^n)^2 + (D_y^0 u^n)^2 + \varepsilon_2}} \\
+ \quad & \min(D_x^0 g, 0) \frac{D_x^+ u^n}{\sqrt{(D_x^0 u^n)^2 + (D_y^0 u^n)^2 + \varepsilon_2}} \\
+ \quad & \max(D_y^0 g, 0) \frac{D_y^- u^n}{\sqrt{(D_x^0 u^n)^2 + (D_y^0 u^n)^2 + \varepsilon_2}} \\
+ \quad & \min(D_y^0 g, 0) \frac{D_y^+ u^n}{\sqrt{(D_x^0 u^n)^2 + (D_y^0 u^n)^2 + \varepsilon_2}} \\
+ \quad & \lambda \frac{u^n - f}{\sqrt{(u^n - f)^2 + \varepsilon_3}}, \qquad (16)
\end{aligned}$$

where $\varepsilon_1, \varepsilon_2, \varepsilon_3$ are small positive constants. In all our experiments, we have chosen $\varepsilon_1 = 10^{-12}$, $\varepsilon_2 = 10^{-4}$ and $\varepsilon_3 = 10^{-4}$.

Let us come back to the first image, Figure 1. However, our new initial guess is more challenging since it is the characteristic function of a small disk outside both objects, see Figure 3. Both objects are now successfully segmented.

The second example is the cameraman picture, Figure 4. This example

illustrates the limitation of the Theorem 1. Indeed, Theorem 1 makes the hypothesis that the given image f is a binary function. Unlike Figure 3 which is a noisy binary function, Figure 4 is very different from a characteristic function. This explains the important differences between the level contours $\mu = 0.4, 0.5$ and 0.6 (which are not global minimizers in this case) observed on Figure 5.

The global minimization of the active contour model is extended to the non-binary image f with the Mumford-Shah model following [4].

3 Global Minimization of the Active Contour Model based on the Mumford-Shah Model

3.1 The Piecewise-Constant Case

In this section we consider the global minimization of the active contour/snake model using the well-known Mumford-Shah functional [12]. Chan and Vese have proposed in [5] the model of *active contours without edges* based on the detection of homogeneous regions. The name of their model underlines well the difference from the standard active contour model based on the detection of edges. We propose to reconcile these two complementary segmentation models in a global minimization framework.

The variational segmentation model of the active contours without edges, i.e. the two-phase piecewise constant Mumford-Shah segmentation model, is as follows:

$$\min_{\Omega_C, c_1, c_2} E_{acwe}(\Omega_C, c_1, c_2) = \mathrm{Per}(\Omega_C) + \lambda \int_{\Omega_C} (c_1 - f(x))^2 \, dx + \lambda \int_{\Omega \setminus \Omega_C} (c_2 - f(x))^2 \, dx, \tag{17}$$

where the region $\Omega_C \subset \Omega$ and $c_1, c_2 \in \mathbf{R}$.
The variational model (17) determines the best approximation, in the L^2 sense of the image f as a set of regions with only two different values, c_1 and c_2. If Ω_C is fixed, the values of c_1 and c_2 which minimize the energy E_{acwe} are the mean values inside and outside Ω_C. Finally the term $\mathrm{Per}(\Omega_C)$ imposes a smoothness constraint on the geometry of the set Ω_C which separates the piecewise constant regions.
The minimization problem (17) is non-convex since minimization is carried

over functions that take only the values c_1 and c_2, which is a non-convex collection. Hence, the optimization problem can have local minima, which implies solutions with wrong scales of details. Despite the non-convex nature of (17), a natural way to determine a solution (Ω_C, c_1, c_2) is a two-step algorithm where c_1 and c_2 are firstly computed, then region Ω_C is updated to decrease the energy E_{acwe}. Chan and Vese have proposed in [5] a solution to determine an evolution equation for the region Ω_C based on a level set based approach. They represent the regions Ω_C and $\Omega \setminus \Omega_C$ with the Heaviside function of a level set function (which models a characteristic function). Hence energy E_{acwe} can be written according to a level set function ϕ:

$$\begin{aligned} E_{CV}(\phi, c_1, c_2) = \int_\Omega |\nabla H_\epsilon(\phi)| + \\ \lambda \int_\Omega H_\epsilon(\phi) \left(c_1 - f(x)\right)^2 + H_\epsilon(-\phi) \left(c_2 - f(x)\right)^2 dx, \end{aligned} \tag{18}$$

where H_ϵ is a regularization of the Heaviside function.
The flow minimizing energy (18) is the following one:

$$\phi_t = H'_\epsilon(\phi) \left\{ \operatorname{div}\left(\frac{\nabla \phi}{|\nabla \phi|}\right) - \lambda \underbrace{\left((c_1 - f(x))^2 - (c_2 - f(x))^2 \right)}_{r_1(x)} \right\}. \tag{19}$$

Chan and Vese [5] have chosen a non-compactly supported smooth strictly monotone approximation of the Heaviside function. As a result, the steady state solution of the gradient flow (19) is the same as:

$$\phi_t = \operatorname{div}\left(\frac{\nabla \phi}{|\nabla \phi|}\right) - \lambda r_1(x), \tag{20}$$

and this equation is the gradient descent flow of the energy:

$$\int_\Omega |\nabla \phi| + \lambda \int_\Omega r_1(x) \phi dx. \tag{21}$$

As explained in [4], this energy is homogeneous of degree 1 in ϕ. This means that this evolution equation does not have a stationary solution if we do not restrict the minimization to ϕ such as $0 \leq \phi(x) \leq 1$.

Based on the work [4], we propose to minimize the following constrained minimization problem for any given observed image $f \in L^1(\Omega)$ and any

positive parameter λ:

$$\min_{0\leq u\leq 1} E_2(u,\lambda) = \int_\Omega g|\nabla u| + \lambda \int_\Omega r_1(x)udx. \tag{22}$$

The relation between the standard active contour model [2, 10] and the model of active contours without edges [5] is as follows: If $\mathbf{1}_{\Omega_C}$ is the characteristic function of a set Ω_C whose boundary is denoted C, then

$$\begin{aligned} E_2(u=\mathbf{1}_{\Omega_C},\lambda) &= \int_\Omega g|\nabla \mathbf{1}_{\Omega_C}| + \lambda \int_\Omega r_1(x)\mathbf{1}_{\Omega_C}dx, & (23)\\ &= \int_C gds + \\ &\quad \lambda \int_\Omega \left((c_1 - f(x))^2 - (c_2 - f(x))^2\right)\mathbf{1}_{\Omega_C}dx. & (24) \end{aligned}$$

Hence, minimizing the energy (24) is equivalent to

$$\textit{minimize} \quad \int_C gds = E_{gac}(C) \quad \text{(the active contour energy (1))}\ ,$$

while

approximating f (in the L^2 sense) by
two regions Ω_C and $\Omega \setminus \Omega_C$ with two values c_1 and c_2.

We state the Theorem 2:

Theorem 2: *Suppose that $f(x), g(x) \in [0,1]$, for any given $c_1, c_2 \in \mathbf{R}$, if $u_\lambda(x)$ is any minimizer of $E_2(.,\lambda)$, then for almost every $\mu \in [0,1]$ we have that the characteristic function*

$$\mathbf{1}_{\Omega_C(\mu)=\{x:u_\lambda(x)>\mu\}}\ (x), \tag{25}$$

where C is the boundary of the set Ω_C, is a global minimizer of $E_2(.,\lambda)$.

Proof. The proof of Theorem 2 is in [4] with the weighted TV-norm replacing the TV-norm.

Finally, the constrained problem (22) becomes an unconstrained minimization problem according to the following theorem given in [4]:

Theorem 3: *Let $r(x) \in L^\infty(\Omega)$. Then the following convex constrained minimization problem*

$$\min_{0\le u\le 1} \int_\Omega g|\nabla u| + \lambda \int_\Omega r(x)u dx \tag{26}$$

has the same set of minimizers as the following convex and unconstrained minimization problem:

$$\min_u \int_\Omega g|\nabla u| + \lambda \int_\Omega \alpha\nu(u) + \lambda r(x)u dx \tag{27}$$

where $\nu(\xi) := \max\{0, 2|\xi - \frac{1}{2}| - 1\}$ provided that $\alpha > \frac{\lambda}{2} \parallel r(x) \parallel_{L^\infty(\Omega)}$.

Proof. The proof is in [4] with the weighted TV-norm replacing the TV-norm.

We look for any minimizer of the convex energy E_2. The Euler-Lagrange technique and the gradient descent based algorithm are used to give us the minimization flow:

$$\begin{aligned} u_t &= \text{div}\left(g\frac{\nabla u}{|\nabla u|}\right) - \lambda r(x) - \alpha\nu'(u), &(28)\\ &= g\ \text{div}\left(\frac{\nabla u}{|\nabla u|}\right) + \langle \nabla g, \frac{\nabla u}{|\nabla u|}\rangle - \lambda r(x) - \alpha\nu'(u), &(29)\end{aligned}$$

where $r(x) = (c_1 - f(x))^2 - (c_2 - f(x))^2$.

Then, we discretize the evolution equation (29) according to the numer-

ical scheme:

$$\begin{aligned}
\frac{u^{n+1}-u^n}{\delta t} = \quad & g(\sqrt{(D_x^0 f_\sigma)^2+(D_y^0 f_\sigma)^2})\cdot \\
& \left\{ D_x^- \left(\frac{D_x^+ u^n}{\sqrt{(D_x^+ u^n)^2+(D_y^+ u^n)^2+\varepsilon_1}} \right) \right. \\
& \left. + D_y^- \left(\frac{D_y^+ u^n}{\sqrt{(D_x^+ u^n)^2+(D_y^+ u^n)^2+\varepsilon_1}} \right) \right\} \\
+ \quad & \max(D_x^0 g, 0) \frac{D_x^- u^n}{\sqrt{(D_x^0 u^n)^2+(D_y^0 u^n)^2+\varepsilon_2}} \\
+ \quad & \min(D_x^0 g, 0) \frac{D_x^+ u^n}{\sqrt{(D_x^0 u^n)^2+(D_y^0 u^n)^2+\varepsilon_2}} \\
+ \quad & \max(D_y^0 g, 0) \frac{D_y^- u^n}{\sqrt{(D_x^0 u^n)^2+(D_y^0 u^n)^2+\varepsilon_2}} \\
+ \quad & \min(D_y^0 g, 0) \frac{D_y^+ u^n}{\sqrt{(D_x^0 u^n)^2+(D_y^0 u^n)^2+\varepsilon_2}} \\
- \quad & \lambda r(x) - \alpha \nu'_{\varepsilon_3}(u), \qquad (30)
\end{aligned}$$

where ν'_{ε_3} is a regularized version of ν' with $\nu_{\epsilon_3}(\xi)$ such that:

$$\nu_{\epsilon_3}(\xi) =$$

$$\begin{cases}
-\xi & \text{if} \quad \xi < -\epsilon_3/\sqrt{2}, \\
(1+\sqrt{2})\xi - \sqrt{\tan^2(3\pi/8)\xi^2 - (\xi-\epsilon_3)^2} & \text{if} \quad -\epsilon_3/\sqrt{2} \le \xi < \epsilon_3, \\
0 & \text{if} \quad \epsilon_3 \le \xi < 1-\epsilon_3, \\
(1+\sqrt{2})\xi - \sqrt{\tan^2(3\pi/8)\xi^2 - (\xi-1+\epsilon_3)^2} & \text{if} \quad -\epsilon_3/\sqrt{2} \le \xi < \epsilon_3, \\
\xi - 1 & \text{if} \quad 1-\epsilon_3 \le \xi.
\end{cases} \qquad (31)$$

In all our experiments, we have chosen $\varepsilon_1 = 10^{-12}$, $\varepsilon_2 = 10^{-4}$ and $\varepsilon_3 = 0.01$.

The minimization flow (29) is applied to the cameraman picture, Figure 6. The two constants c_1 and c_2 are updated every 50 iterations. The final solution (Figure 6(d)) is close to a binary function which gives us, according to Theorem 2, similar global minimizers as we can observe on Figure 7.

3.2 The Piecewise-Smooth Case

We extend the result of Section 3.1 to the two-phase piecewise *smooth* Mumford-Shah segmentation model. In this situation, the variational problem to solve is given in [18] by:

$$\begin{aligned}\min_{\Omega_C,s_1,s_2} E_{MS_{2phase}}(\Omega_C,s_1,s_2) = \mathrm{Per}(\Omega_C)+ \\ \lambda\int_{\Omega_C}(s_1(x)-f(x))^2+\mu|\nabla s_1(x)|^2dx \\ \lambda\int_{\Omega\setminus\Omega_C}(s_2(x)-f(x))^2+\mu|\nabla s_2(x)|^2dx,\end{aligned} \tag{32}$$

where the region $\Omega_C \subset \Omega$ and s_1 and s_2 are two C^1 functions on Ω_C and on $\Omega \setminus \Omega_C$ respectively.
The variational problem (32) determines the best approximation, in the L^2 sense, of the image f as a set of smooth regions represented by the function $s(x)$ such that

$$s(x) = \begin{cases} s_1(x) \text{ if } x \in \Omega_C, \\ s_2(x) \text{ if } x \in \Omega \setminus \Omega_C, \end{cases} \tag{33}$$

and $C = \partial\Omega_C$ is the boundary between the smooth regions.
As (17), the minimization problem (32) is also non-convex, which implies the existence of local minima and possible unsatisfactory segmentation results.
As in the previous section, both regions Ω_C and $\Omega \setminus \Omega_C$ are represented by the Heaviside function of a level set function. This leads to the following energy:

$$\begin{aligned}E_{CV_2}(\Omega_C,s_1,s_2) = \int_\Omega |\nabla H_\epsilon(\phi)|+ \\ \lambda\int_\Omega H_\epsilon(\phi)((s_1-f)^2+\mu|\nabla s_1|^2)dx \\ \lambda\int_\Omega H_\epsilon(-\phi)((s_2-f)^2+\mu|\nabla s_2|^2)dx.\end{aligned} \tag{34}$$

Minimizing E_{CV_2} with respect to the functions s_1 and s_2 using the calculus of variations gives us:

$$\begin{cases} s_1 - f = \mu\Delta s_1 \text{ in } \Omega_C, \\ s_2 - f = \mu\Delta s_2 \text{ in } \Omega \setminus \Omega_C, \end{cases} \tag{35}$$

with the Neumann boundary conditions:

$$\begin{cases} \frac{\partial s_1}{\partial \vec{N}} = 0 \text{ on } \partial\Omega_C \cup \partial\Omega, \\ \frac{\partial s_2}{\partial \vec{N}} = 0 \text{ on } \partial(\Omega \setminus \Omega_C) \cup \partial\Omega. \end{cases} \tag{36}$$

And the flow minimizing the energy (34) is as follows:

$$\begin{aligned} \phi_t &= H'_\epsilon(\phi)\{\operatorname{div}\left(\frac{\nabla\phi}{|\nabla\phi|}\right) - \\ &\quad \underbrace{\lambda\left((s_1 - f)^2 - (s_2 - f)^2 + \mu|\nabla s_1|^2 - \mu|\nabla s_2|^2\right)}_{r_2(x)}\} \end{aligned} \tag{37}$$

If a non-compactly supported smooth approximation of the Heavide function is chosen, the steady state solution of the gradient flow (37) is the same as:

$$\phi_t = \operatorname{div}\left(\frac{\nabla\phi}{|\nabla\phi|}\right) - \lambda r_2(x) \tag{38}$$

and this equation is the gradient descent flow of the energy:

$$\int_\Omega |\nabla\phi| + \lambda \int_\Omega r_2(x)\phi dx. \tag{39}$$

As a result, the following constrained minimization problem is proposed for any given image $f \in L^1(\Omega)$ and any positive parameter λ :

$$\min_{0\le u\le 1} E_3(u, \lambda) = \int_\Omega g|\nabla u| + \lambda \int_\Omega r_2(x) u dx. \tag{40}$$

We point out that in formulation (34) of the piecewise smooth functional the two functions s_1 and s_2 need to be defined only on their respective domains (namely Ω_C and $\Omega \setminus \Omega_C$) because of the Heaviside function. However, in the relaxed formulation given in (40), these functions need to be defined in the entire domain Ω (by a suitable extention).

The relation between the standard active contour model [2, 10] and the model of active contours based on the 2-phase Mumford-Shah functional [18] is as follows:

$$E_3(u = \mathbf{1}_{\Omega_C}, \lambda) = \int_\Omega g|\nabla \mathbf{1}_{\Omega_C}| + \lambda \int_\Omega r_2(x)\mathbf{1}_{\Omega_C} dx, \tag{41}$$

$$\begin{aligned} &= \int_C g ds + \\ &\lambda \int_\Omega \left((s_1 - f)^2 - (s_2 - f)^2 + \mu|\nabla s_1|^2 - \mu|\nabla s_2|^2\right)\mathbf{1}_{\Omega_C} dx. \end{aligned} \tag{42}$$

Hence, minimizing the energy (24) is equivalent to

$$\textit{minimize} \quad \int_C g ds = E_{gac}(C) \quad \text{(The active contour energy (1))} \ ,$$

while

$$\begin{array}{c} \text{approximating } f \text{ (in the } L^2 \text{ sense) by} \\ \text{two piecewise smooth regions } \Omega_C \text{ and } \Omega \setminus \Omega_C. \end{array}$$

We state Theorem 4:

Theorem 4: *Suppose that $f(x), g(x) \in [0,1]$, for any given $s_1 \in C^1(\Omega)$, $s_2 \in C^1(\Omega)$, if $u_\lambda(x)$ is any minimizer of $E_3(., \lambda)$, then for almost every $\mu \in [0,1]$ we have that the characteristic function*

$$\mathbf{1}_{\Omega_C(\mu)=\{x:u_\lambda(x)>\mu\}} \ (x), \tag{43}$$

where C is the boundary of the set Ω_C, is a global minimizer of $E_3(., \lambda)$.

Proof. The proof of Theorem 4 is similar to the proof of Theorem 2.

And finally, the constrained problem (40) becomes an unconstrained minimization problem according to the Theorem 3, Section 3.1.

A minimizer of the convex energy E_3 can be found using the following minimization flow:

$$u_t = \operatorname{div}\left(g\frac{\nabla u}{|\nabla u|}\right) - \lambda r_2(x) - \alpha\nu'(u), \tag{44}$$

with $\alpha > \frac{\lambda}{2} \parallel r_2(x) \parallel_{L^\infty(\Omega)}$.

The previous minimization flow is applied to the cameraman picture, Figure 8. The two functions s_1 and s_2 are initially chosen to f and updated every 10 iterations according to Equation (35). The final solution (Figure 8(e)) is close to a binary function which gives us, according to Theorem 4, similar global minimizers.
We have also segmented (Figure 9(f)) and denoised (Figure 9(b)) a piecewise smooth image (Figure 9(a)). And finally we have applied our segmentation/denoising model to the galaxy picture on Figure 10.

4 Conclusion

In this paper, we have proposed three algorithms to find global minimizers of the active contour/snake variational model following the approach of Chan, Esedoḡlu and Nikolova [4, 3]. The first algorithm, defined from the ROF model, determines global minimizers of the snake model for any observed image close to a binary function. The two other algorithms, based on the Chan-Vese version of the Mumford-Shah model, find global minimizers (when parameters c_1, c_2 or functions s_1, s_2 are fixed) for any type of images, binary or non-binary.
It will not be surprising to see new applications of the approach introduced in [4, 3] to other image processing models to get global minima. The key idea is to express the energy functionals in terms of level sets as observed by Strang [16, 17].
In this work, we have determined not one but several global minimizers of the active contour model, which looks to be a drawback. However, all global solutions are reasonable solutions and most of them are close to each other. From a numerical point of view, the three algorithms are slow even if the standard re-initialization process of the level set function is not used in this approach. The non-linear nature of our PDEs requires to use a very small temporal step to guarantee a consistent evolution process. However, fast numerical schemes can be used to speed up the algorithms such as the second-order cone programming algorithm [1].
Let us finally mention the paper [7] of Cohen and Kimmel which also addresses the problem of determining a global minimum for the active contour model's energy. However, their approach is different from ours since it is focused on finding a minimal path between two given end points of an open curve. They have extended their method to closed curves but a topology-based saddle search routine is needed.

References

[1] F. Alizadeh and D. Goldfarb. Second-Order Cone Programming, Technical Report 51-2001, RUTCOR, Rutgers University, 2001.

[2] V. Caselles, R. Kimmel, and G. Sapiro. Geodesic Active Contours. *International Journal of Computer Vision*, 22(1):61–79, 1997.

[3] T.F. Chan and S. Esedoḡlu. Aspects of Total Varation Regularized L^1 function Approximation, UCLA CAM Report 04-07, 2004.

[4] T.F. Chan, S. Esedoḡlu, and M. Nikolova. Algorithms for Finding Global Minimizers of Image Segmentation and Denoising Models, UCLA CAM Report 04-54, 2004.

[5] T.F. Chan and L.A. Vese. Active Contours Without Edges. *IEEE Transactions on Image Processing*, 10(2):266–277, 2001.

[6] E. Cheon and A. Paranjpye. Noise removal by total variation minimization, UCLA MATH 199 project report, adviser: L. Vese, 2002.

[7] L.D. Cohen and R. Kimmel. Global Minimum for Active Contour Models: A Minimal Path Approach. *International Journal of Computer Vision*, 24(1):57–78, 1997.

[8] L. Jonasson, X. Bresson, P. Hagmann, O. Cuisenaire, R. Meuli, and J.P. Thiran. White Matter Fiber Tract Segmentation in DT-MRI Using Geometric Flows. *Medical Image Analysis*, In Press, 2004.

[9] M. Kass, A. Witkin, and D. Terzopoulos. Snakes: Active Contour Models. *International Journal of Computer Vision*, pages 321–331, 1987.

[10] S. Kichenassamy, A. Kumar, P. Olver, A. Tannenbaum, and A.J. Yezzi. Conformal Curvature Flows: From Phase Transitions to Active Vision. In *Archive for Rational Mechanics and Analysis*, volume 134, pages 275–301, 1996.

[11] R. Malladi, R. Kimmel, D. Adalsteinsson, G. Sapiro, V. Caselles, and J.A. Sethian. A Geometric Approach to Segmentation and Analysis of 3D Medical Images. In *Mathematical Methods in Biomedical Image Analysis Workshop*, 1996.

[12] D. Mumford and J. Shah. Optimal Approximations of Piecewise Smooth Functions and Associated Variational Problems. *Communications on Pure and Applied Mathematics*, 42:577–685, 1989.

[13] S. Osher. *"Level Set Methods", in Geometric Level Set Methods in Imaging, Vision and Graphics.* eds. S. Osher and N. Paragios, Springer-Verlag, NY, 2003.

[14] S. Osher and J.A. Sethian. Fronts Propagating with Curvature-Dependent Speed: Algorithms Based on Hamilton-Jacobi Formulations. *Journal of Computational Physics*, 79(1)(12-49), 1988.

[15] L. I. Rudin, S. Osher, and E. Fatemi. Nonlinear Total Variation Based Noise Removal Algorithms. *Physica D*, 60(1-4):259 – 268, 1992.

[16] G. Strang. L^1 and L^∞ Approximation of Vector Fields in the Plane. In *Nonlinear Partial Differential Equations in Applied Science*, pages 273–288, 1982.

[17] G. Strang. Maximal Flow Through A Domain. *Mathematical Programming*, 26(2):123–143, 1983.

[18] L.A. Vese and T.F. Chan. A Multiphase Level Set Framework for Image Segmentation Using the Mumford and Shah Model. *International Journal of Computer Vision*, 50(3):271–293, 2002.

[19] L.A. Vese and S.J. Osher. The Level Set Method Links Active Contours, Mumford-Shah Segmentation, and Total Variation Restoration, UCLA CAM Report 02-05, 2002.

[20] A.Jr. Yezzi, S. Kichenassamy, A. Kumar, P.J. Olver, and A. Tannenbaum. A Geometric Snake Model for Segmentation of Medical Imagery. *IEEE Transactions on Medical Imaging*, 16(2):199–209, 1997.

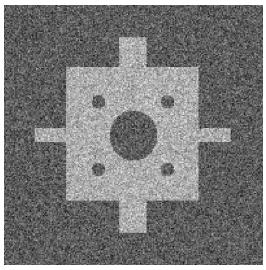

(a) Original image.

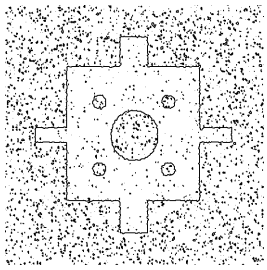

(b) Initial $\partial\{x : u(x) > 0.5\}$.

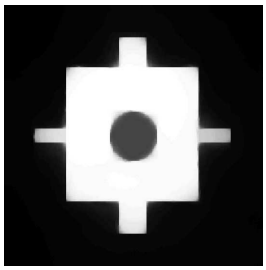

(c) Final u (TV-L^1).

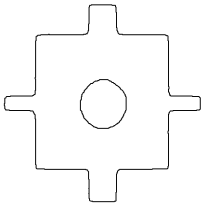

(d) Final $\partial\{x : u(x) > 0.5\}$ (TV-L^1).

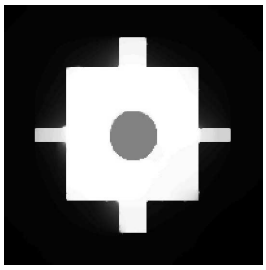

(e) Final u (weighted TV-L^1).

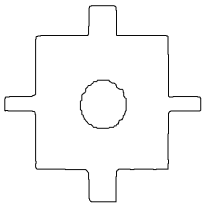

(f) Final $\partial\{x : u(x) > 0.5\}$ (weighted TV-L^1).

Figure 2: Comparison between the ROF model with L^1-norm as a fidelity measure and our model defined by the weighted TV-norm and the L^1-norm. The difference between both models is clear. The result generated by our model better preserves the geometry of the original features such as the corners and the largest circle.

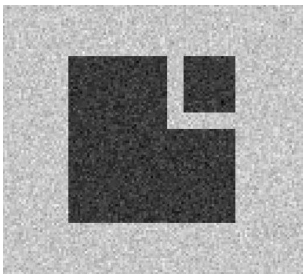

(a) Original image.

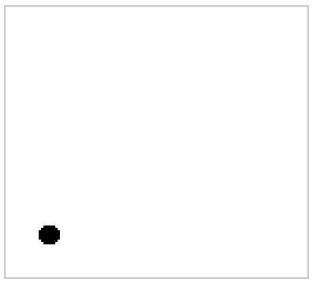

(b) Initial u.

(c) Initial $\partial\Omega_C(\mu = 0.5)$.

(d) Final u.

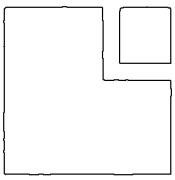

(e) Final $\partial\Omega_C(\mu = 0.5)$.

Figure 3: Our segmentation/denoising model has successfully extracted both objects (Figure 3(e)) in the noisy image (Figure 3(a)) whereas the initial guess (Figure 3(c)) was a small circle outside both objects. This improves the standard active contour result obtained on Figure 1 where a good initial guess is needed to get the same result.

(a) Original image.

(b) Initial u.

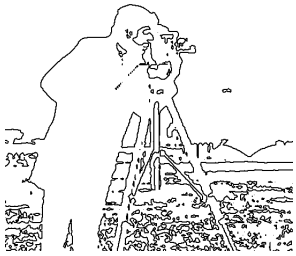

(c) Initial $\partial\Omega_C(\mu = 0.5)$.

(d) Final u.

(e) Final $\partial\Omega_C(\mu = 0.5)$.

Figure 4: Figure 4(e) presents the result obtained by the minimization the energy E_1. This example illustrates the limitation of the Theorem 1 which makes the hypothesis that the observed image f is a binary function. Since this condition is not respected here, we get different level contours (which are not global minimizers) as we can observe on Figure 5.

(a) Final $\partial\Omega_C(\mu = 0.5)$.

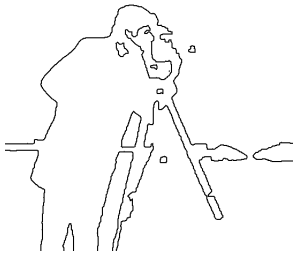

(b) Final $\partial\Omega_C(\mu = 0.4)$.

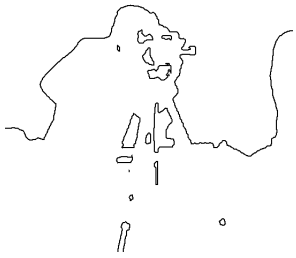

(c) Final $\partial\Omega_C(\mu = 0.6)$.

Figure 5: Since the cameraman picture is not a binary function, different level contours (which are not global minimizers) are obtained for $\mu = 0.4, 0.5$ and 0.6.

(a) Original image.

(b) Initial u.

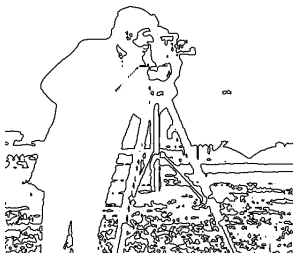

(c) Initial $\partial\Omega_C(\mu = 0.5)$.

(d) Final u.

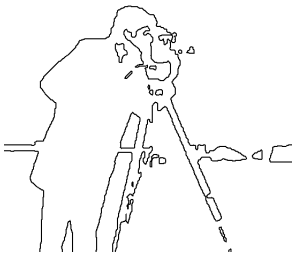

(e) Final $\partial\Omega_C(\mu = 0.5)$.

Figure 6: Figure 6(e) presents the contour obtained by the global minimization of the active contour energy subject to an intensity homogeneity constraint based on the Mumford-Shah energy (the 2-phase piecewise constant case defined in [5]). Our global minimization approach allows us to reconcile the standard active contour model with the model of Active Contours Without Edges.

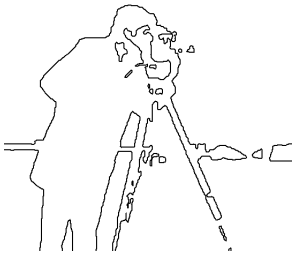

(a) Final $\partial\Omega_C(\mu = 0.5)$.

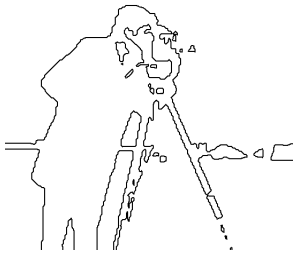

(b) Final $\partial\Omega_C(\mu = 0.4)$.

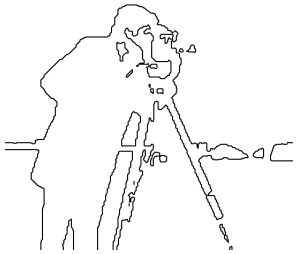

(c) Final $\partial\Omega_C(\mu = 0.6)$.

Figure 7: Unlike Figure 5 where level contours are different from each other since the given image is not binary, the level lines of Figure 6(d) are similar and correspond to global minimizers.

(a) Original image.

(b) Piecewise-smooth approximation.

(c) Initial u.

(d) Initial $\partial\Omega_C(\mu = 0.5)$.

(e) Final u.

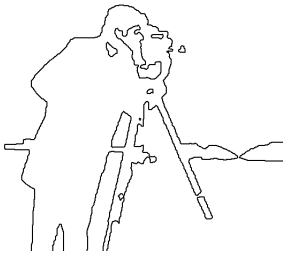

(f) Final $\partial\Omega_C(\mu = 0.5)$.

Figure 8: Figure 8(f) presents the contour obtained by the global minimization of the active contour energy subject to an intensity homogeneity constraint based on the Mumford-Shah energy (the 2-phase piecewise smooth case defined in [18]). Our global minimization approach allows us to reconcile the standard active contour model with the model of Active Contours based on the Mumford-Shah approach. Finally, Figure 8(b) shows the best piecewise smooth approximation of the original image (Figure 8(a))

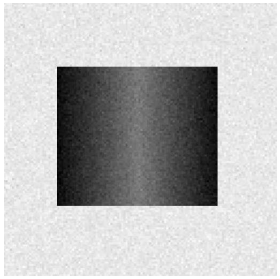

(a) Original image.

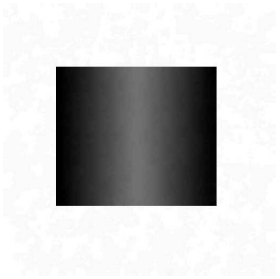

(b) Piecewise-smooth approximation.

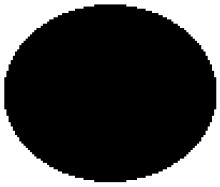

(c) Initial u.

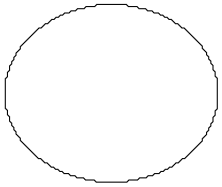

(d) Initial $\partial\Omega_C(\mu = 0.5)$.

(e) Final u.

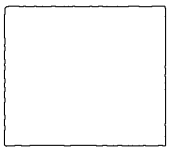

(f) Final $\partial\Omega_C(\mu = 0.5)$.

Figure 9: Figure 9(f) presents the contour obtained by the global minimization of the active contour energy subject to an intensity homogeneity constraint. Figure 9(b) shows the best piecewise smooth approximation of the original image (Figure 9(a)).

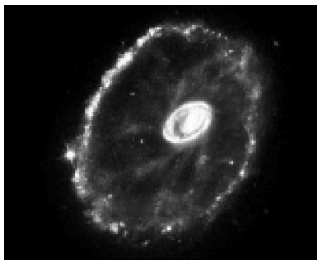

(a) Original image.

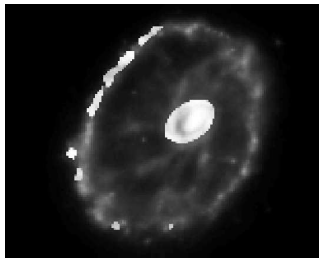

(b) Piecewise-smooth approximation.

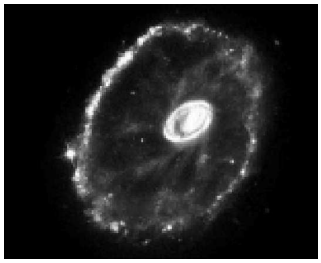

(c) Initial u.

(d) Initial $\partial\Omega_C(\mu = 0.5)$.

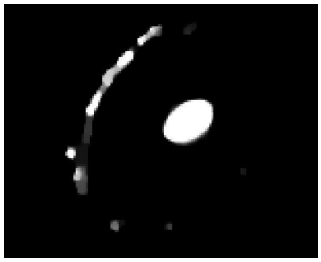

(e) Final u.

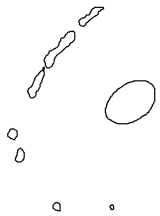

(f) Final $\partial\Omega_C(\mu = 0.5)$.

Figure 10: Figure 10(f) presents the contour obtained by the global minimization of the active contour energy subject to an intensity homogeneity constraint. Figure 10(b) shows the best piecewise smooth approximation of the original image (Figure 10(a)).